第 48 卷 第 10 期
2021 年 10 月

湖南大学学报（自然科学版）
Journal of Hunan University（Natural Sciences）

Vol. 48 No. 10
October 2021

Computer-Assisted Framework for Automatic Detection of Structural Hand Deformities

Madeha Muzafar Memon*, Muhammad Moazzam Jawaid, Sanam Narejo, Mahaveer Rathi

Department of Computer Systems Engineering, Mehran University of Engineering & Technology, Jamshoro, 71000, Pakistan

Abstract: The hand is the most complex and important prehensile organ in the human skeleton. Deformities in any phalange of hand effects the reduction of everyday routine work and job loss. This research aims to propose an efficient method that automatically detects various hand abnormalities using different mathematical and morphological image processing techniques before treatment, as detecting short bones abnormalities is extremely challenging for orthopedics. Therefore, we investigated five congenital and acquired abnormalities, including enumeration of fingers, absence of phalanges, angle computation between the fingers, finger flexion from normal trend, and fracture computation on 950 hand radiographs obtained from MURA. Statistical parameters were evaluated to obtain precision, specificity, sensitivity and achieved 95.95% accuracy.

Keywords: medial axis transform, skeletonization, image, morphology, segmentation.

自动检测手部结构畸形的计算机辅助框架

摘要: 手是人体骨骼中最复杂、最重要的抓握器官。 任何指骨的畸形都会影响日常工作和失业的减少。本研究旨在提出一种有效的方法，在治疗前使用不同的数学和形态学图像处理技术自动检测各种手部异常，因为检测短骨异常对骨科而言极具挑战性。 因此，我们研究了五种先天性和获得性异常，包括手指计数、指骨缺失、手指之间的角度计算、正常趋势的手指屈曲以及从村获得的 950 张手部 X 光片的骨折计算。 对统计参数进行评估以获得精确度、特异性、灵敏度并达到 95.95% 的准确度。

关键词：中轴变换、骨架化、图像、形态学、分割。

1. Introduction

The most complex prehensile structure in the human body is the hand. It is divided into three segment bones forming a shape of five fingers localized at the forearm. Phalanges are the first topmost segment consisting of fourteen bones [1]. Each finger consists of three phalanges possessing distal inter phalanges, middle inter phalanges, and proximal inter phalanges, except the thumb that does not have middle inter phalange bone. Metacarpals are the second segment in the hand containing five bones, and carpals are the third segment having eight small bones, also called wrist bones, which join the forearm [2].

1.1. Clinical Motivation

The ratio of hand deformities is escalating in all emergency wards as the hand is a frequently used organ in everyday job routines. According to the prevalence rate registry of structural deformities, hand deformities account for about 40% of overlying extremity fractures [3]. The most common congenital abnormalities are polydactyly and syndactyly, of about 23.4 per 10,000 newborns. The frequency of dislocation of metacarpal bones is 89% in athletes of sports such as arm wrestling, boxing, and pull-ups [4]. Furthermore, a fall onto an outstretched hand (FOOSH) often occurs in old age and childhood by losing the balance of the body, causing wrist bone fractures, especially of the lunate and scaphoid bones [5].

Before treatment, the detection of bone fractures and other deformities is a prime challenge as conventional

Received: June 3, 2021 / Revised: August 1, 2021 / Accepted: September 4, 2021 / Published: October 30, 2021

About the authors: Madeha Muzafar Memon, Muhammad Moazzam Jawaid, Sanam Narejo, Mahaveer Rathi, Department of Computer Systems Engineering, Mehran University of Engineering & Technology, Jamshoro, Pakistan

Corresponding author Madeha Muzafar Memon, madeha.memon@faculty.muet.edu.pk

radiography requires orthopedic doctors who have specialized knowledge of bone deformities, which is not widely available. Therefore, to overcome the inefficient manual interpretation of hand X-ray images and to reduce the time and efforts to hire and train physicians, a computer-aided research study is presented in this paper to detect malformations from hand radiographic images using various image processing techniques.

2. Literature Review

With the advancement of technology in medical science, the detection of long bone abnormalities now requires less effort, whereas deformities of small hand bones are still challenging problems to interpret; hence, only few research studies are available on this topic. Zare et al. [6] proposed a content-based image retrieval method for extracting bone fractures using low-level features, such as the boundary of the bones and shape curvature, using canny edge detection and gray-level co-occurrence techniques to classify X-ray images. Chai et al. [7] has contributed to detecting fractures of the longest femur bone of the lower limbs of the body using a gray-level co-occurrence matrix method by selecting a fixed GLCM parameter of 0.95 units on a few images; the method detects the presence and absence of cracks in the femur bone. Al-Ayyoub et al. [8] used multi-level meta-classifiers to detect bone fractures in hand radiographs. Initially, they pre-processed the radiographs and then applied Bayesian network classifiers by using boosting and bagging techniques. A feature set was determined by applying a gray-level co-occurrence matrix and curvelet and wavelet transforms for detecting only phalange fractures. Al-Ayyoub et al. [9] proposed an automatic method to detect fractures from lower limb radiographs. The pre-processed radiographs were further employed in the support vector machine algorithm, which splits margin into the fractured and non-fractured data points as the presence and absence of leg fracture. Bhisikar et al. [10] have thoroughly assessed osteoarthritis of hand radiographs. Gaussian filtering and binarization techniques were implemented to assess the normal spaces between each of the bones. Tripathi [11] carried out morphological operations which highlighted the foreground pixels to detect the edges of bones. Subsequently, the processed images were used in the support vector machine algorithm to differentiate the fractured femur bone. Johari N et al. [12] develop an automatic system to detect bone fracture using a canny edge detector. Initially, x-ray images were pre-processed using a Gaussian filter to remove extra lines from images. However, the approach worked only for sigma 4.75 value by selecting the threshold for sobel edge detection for transverse fracture position.

3. Research Methodology

This paper incorporates various image processing techniques and mathematical formulations for detecting number of hand abnormalities, including enumeration of finger, angle computation between the fingers, finger flexion from normal trend, missing of upper phalanges and fracture detection which is implemented on Matlab 2018a.The general diagram to detect hand malformations is presented in Fig. 1.

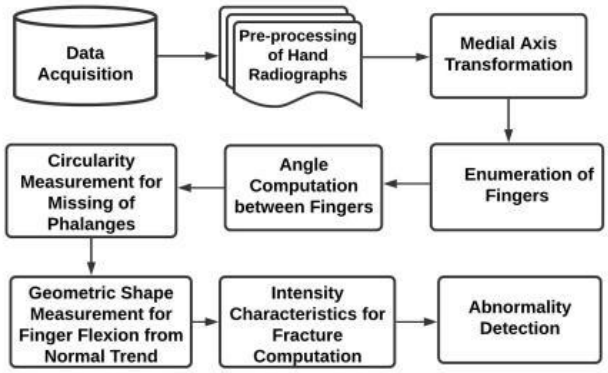

Fig. 1 Research methodology flowchart

3.1. Data Acquisition

The hand radiographs are obtained from MURA (Muscular radiographic) images in DICOM format, which is converted to JPG format having 406 x 512 spatial resolution [13]. Lateral, Oblique, and Posterior anterior view radiographs are ground truth labeled as positive for abnormal and negative for normal radiographs. The dataset contains total of 2100 radiographs for around 500 patients having 700 abnormal images and 1400 normal images.

3.2. Pre-Processing of Radiographs

Before extracting the region of interest, the initial step is to remove the noise from each of the hand radiographs, which sharpens and enhances the useful information.

3.3. Otsu Thresholding Method for Segmentation

Segmentation refers to fractionating an image into meaningful segments [22]. Otsu thresholding method segments images by returning threshold intensity in bimodal way for foreground and background [14].

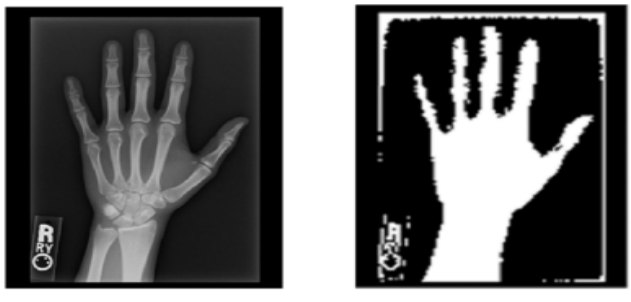

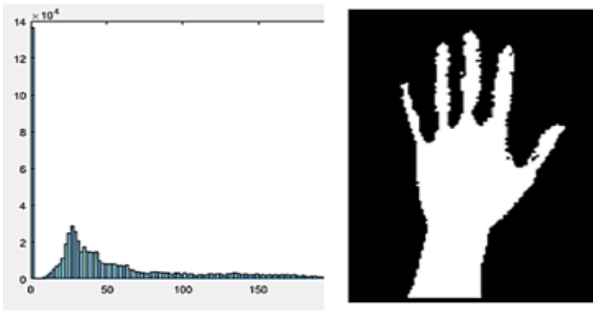

Fig. 2 Segmentation of normal hand X-ray: (a) the normal hand x-ray, (b) the pre-processed radiograph, (c) the histogram having three modes, (d) the segmented region of interest

The histogram exhibits three intensity values for connected objects in the foreground. The first brighter object is the border of x-ray image, the second brighter object is the region of interest hand, and the third brighter object is the label. The results of the histogram exhibiting three intensity values are retaining the intensity range from 11 to 70 for the region of interest and segregating the border and label from radiograph.

3.4. Enumeration of Fingers

Polydactyly, syndactyly, and radial polydactyly are elementary abnormalities of the human hand, having more or less than five digits, which can be congenital or acquired [15]. The number of finger digits is counted using medial axis transform method.

3.5. Medial Axis Transform

In shape morphology, medial axis transform, also known as skeleton thinning algorithm [16-19], is applied to the pre-processed hand radiographs, which shrinks the closest pixels of fingers by generating a central skeleton thinning line by preserving the original shape of fingers as expressed in Eq. (1).

$$A \circ B = b\varepsilon B \quad A_b \tag{1}$$

where A is the preprocessed hand radiograph, B is the structuring element of order 3 x 3, and b is the translation of image A. The skeleton method erodes the extra pixels of fingers by confining them to generate branches as the central line. Therefore, the number of branches enumerates the normal finger count in hand.

Fig. 3 Abnormal finger count: (a) patient radiograph having syndactyly abnormality, (b) the patient having polydactyly syndrome, (c) severe polydactyly syndrome of the patient

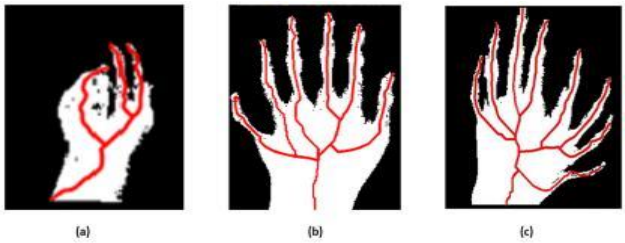

Fig. 4 Finger count results: (a) three-digit abnormal count using skeletonization on pre-processed syndactyly radiograph, (b) six-digit finger count on preprocessed polydactyly syndrome radiograph, (c) eight-digit finger count polydactyly abnormality

3.6. Angle Computation between the Fingers

One of the most common abnormalities in athletes and sportsmen is angle displacement between the fingers [20]. According to a study by orthopedic surgeons [21], the normal angle between the fingers comprising distal inter phalanges, proximal inter phalanges, and metacarpal inter phalanges is measured based on carpometacarpal (CMC) and trapeziometacarpal (TMC) base points forming an angle between the thumb and the index finger of ≤ 25°, between the thumb and the middle finger of ≤ 39°, between the thumb and the ring finger of ≤ 49°, and between the thumb and the small finger of ≤ 69°.

Angle between the finger = (acos(sum(dv1 x dv2)))/(norm(dv1) x norm(dv2)) (2)

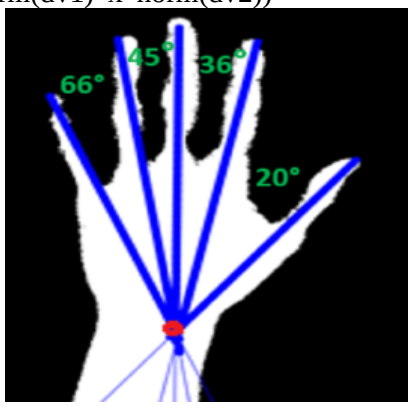

Fig. 5 Normal angle computation of right-hand radiograph

The corresponding angle between the thumb and index finger is computed by calculating the direction vectors dv1 and dv2 for both fingers, respectively, by selecting the reference point of the scaphoid bone, which is the centermost bone of the wrist up to the tip of each finger (Eq. (2)). Similarly, dv2 is a direction vector for the thumb, which remains the same for measuring corresponding angles between the thumb and middle finger, the thumb and ring finger, and the thumb and small finger, respectively.

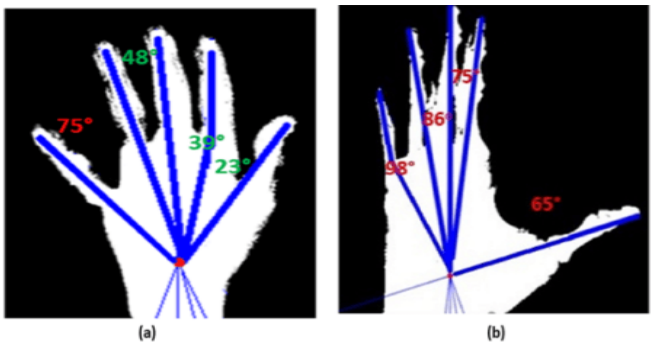

Fig. 6 Abnormal finger computation: (a) a small finger making an abnormal angle, (b) all fingers making an abnormal angle with the thumb

The index, middle, and ring fingers in Fig. 6(a) form a normal angle with the thumb. However, the small finger exceeds the normal angle range, which is categorized as an abnormality. Subsequently, in Fig. 6(b), when the thumb being the reference point is dislocated from the origin of the scaphoid bone, it makes all the fingers displaced. Thus, all the fingers make abnormal angles from the metacarpal, carpal to phalanges.

3.7. Absence of Finger Phalanges

Every finger comprises three joints, DIP, PIP, MCP, except the thumb containing only two bones. For measuring the completeness of the hand radiograph, circularity is computed. The normal circularity containing all fourteen bones equals 1.

3.8. Circularity Computation

The integrity of the upper phalanges is computed by selecting the top point of the DIP bone of each finger, from the thumb to the index finger, middle finger, ring finger, and small finger. Subsequently, a closed curve is formed by marking the reference line from the thumb to the end of the small finger, which provides a clone of the upper phalanges to measure the completeness of the hand bones.

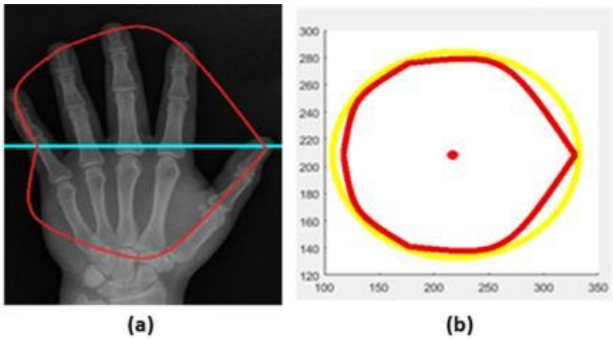

Fig. 7 Circularity measurement for a normal radiograph: (a) enclosed polygon of a normal radiograph, (b) circularity computation result of normal radiograph

The circularity of a complete circle is 1. Therefore, the circularity of the hand radiograph is computed by Eq. (3). The circularity computed for a normal hand radiograph is C = 0.91 units, which is approximately equal to 1. Thus, the enclosed polygon conserves the shape of the circle and denotes it to be normal, which means each of the phalanx bone's proximal interphalangeal, distal interphalangeal and metacarpal interphalangeal bones are present in the hand radiograph.

$$\text{Circularity} = \frac{4 \text{ x pi x area}}{\text{Perimeter}^2} \quad (3)$$

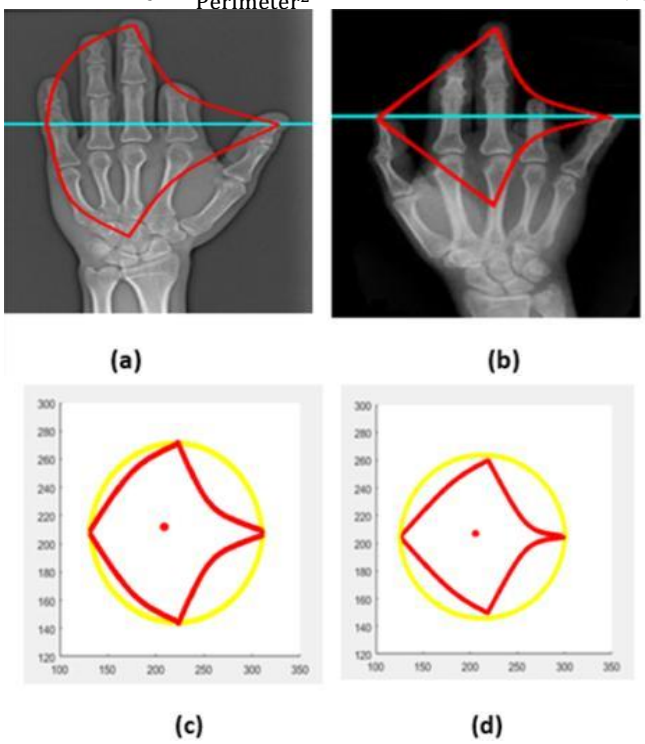

Fig. 8 Circularity measurement for abnormal radiograph: (a) the absence of index finger DIP and PIP bones, (b) the absence of small and ring finger PIP bones, (c) C = 0.72 absence of DIP and PIP bones, (d) C = 0.67 absence of PIP bones

Afterward, taking all finger points for the right hand and forming a closed curve, as in Fig. 8(a), the circularity computed is C = 0.72, which exhibits the absence of the distal interphalangeal and proximal interphalangeal bones of the index finger. Similarly, for the left hand circularity is C = 0.67, which illustrates the absence of the DIP and PIP bones of the ring finger.

3.9. Standard Deviation

Another technique to measure the completeness of phalanges in the hand is to calculate the total dispersion, or variation, from the actual data. The lower the dispersion rate, the closer the points are to their mean value. Similarly, the higher the dispersion rate, the further the points are from the mean value.

$$\text{S. D} = \sqrt{\frac{1}{N} \sum_{i=1}^{N} (xi - \mu)^2} \quad (4)$$

The dispersion rate of points in a finger is expressed by Eq. (4). Initially, the length of each finger is calculated from the tip of each finger's DIP bone to the end of each finger by using the distance formula. Subsequently, standard deviation is computed where μ is the mean value of each phalanx, N is the finger count, and xi is the total distance of all phalanges.

3.10. Finger Flexion from Normal Trend

Hypermobility syndrome, or finger flexion beyond normal trend, is another hand deformity in which the finger gets bent or stretched from its actual shape [21]. Finger flexion is computed using mathematical and morphological formulas. Initially, each finger is skeletonized using medial axis transform, which erodes the boundaries of the fingers and the linear line is generated from the tip to the end of each finger as expressed in Eq. (5).

Linear Line = z = ax + b (5)

where a = $\frac{v2 - v1}{u2 - u1}$ and u_1 and v_1 are the starting points of the finger. Similarly, u_2 and v_2 are the ending points of the finger.

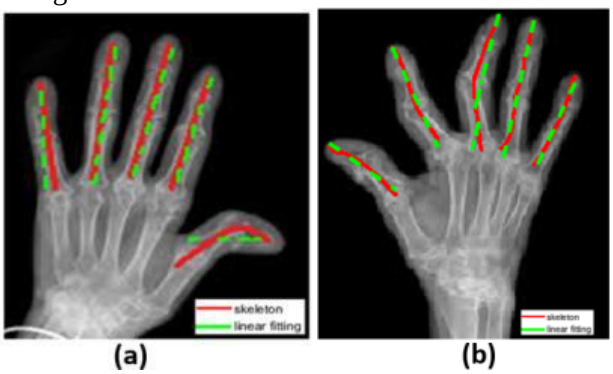

Fig. 9 Skeleton and linear line fitting for finger flexion: (a) thumb bending from normal trend, (b) middle and index finger bending from the normal trend

After calculating the skeleton and linear lines for each of the fingers, the next step is to measure the distance from each skeleton point to each point in the linear line as expressed in Eq. (6). The maximum number of points are in the middle finger since it is the largest finger in hand. Therefore, it helps to determine the range for selecting the total number of points for each finger to generate the skeleton and linear lines.

$$d = \sqrt{(u_2 - u_1)^2 + (v_2 - v_1)^2)} \quad (6)$$

The distance for each finger is measured by taking each skeleton point and each linear line point, respectively. Thus, dispersion error exhibits the dispersal rate or distance rate of the skeleton and linear line points. Normal fingers show a low dispersal rate, and abnormal fingers show a high dispersal rate.

4. Fracture Computation

Bone cracks or fractures are among the most frequent injuries to the bones of the hand. Hand fractures are detected using the linear interpolation image processing technique.

4.1. Linear Interpolation

The intensity and slope of each finger are determined to compute the linear interpolation technique. Initially, the intensity of the little finger is measured, and an intensity profile is generated. Similarly, all intensity profiles for each finger are saved.

$$y - y_1 = \frac{y_2 - y_1}{x_2 - x_1}(x - x_1) \quad (7)$$

$$m = \frac{y_2 - y_1}{x_2 - x_1} \quad (8)$$

where the intercept points are x and y, the first tip points of the finger are x_1 and y_1, and the second tip points of the finger are x_2 and y_2.

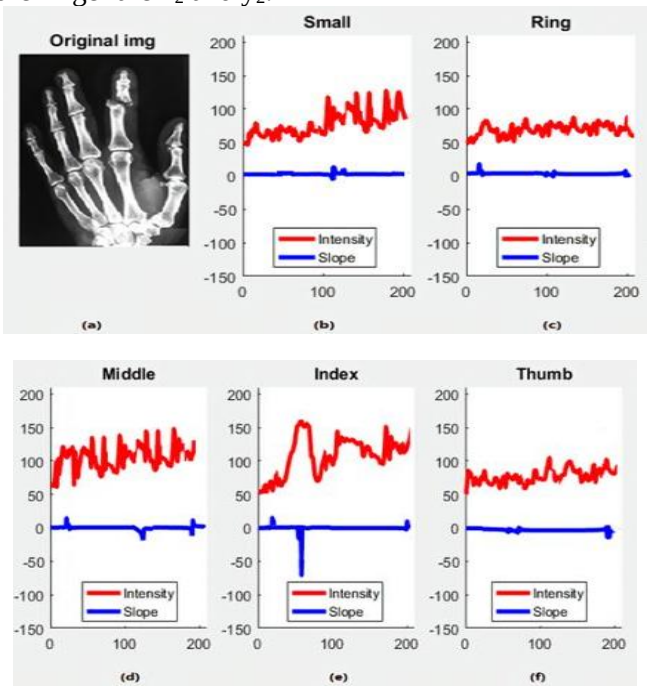

Fig. 10 Fracture detection of hand radiograph: (a) preprocessed hand x-ray, (b) intensity and slope variation of the small finger, (c) intensity and slope variation of the ring finger, (d) intensity and slope variation of the middle finger, (e) a radical change in intensity and slope of the index finger, (f) the intensity and slope variation of the thumb

Anatomically, every finger has a gap between each of the phalanges. The intensities vary with a small change when there is a gap between the fingers, but the slope remains constant. The intensities for the thumb, middle, ring and little fingers vary slightly, whereas there is no change in the slope. However, a radical change occurs in intensities and in the slope of the index finger which shows the breakage of the bone (Fig. 10(d)).

5. Results

5.1. Enumeration of the Fingers

To verify the results for each of the abnormalities using different image processing and morphological techniques, the first step is to investigate the evidence for all the hand radiographs, which are labeled. The corresponding labels show the status of the radiograph— normal is negative (0), and abnormal is positive (1).

Table 1 Results of the enumeration of fingers

P_ID	Ground truth evidence	Finger Count
Continuation of Table 1		
P0712	Positive	3
P0786	Negative	5
P0901	Positive	6
P0529	Positive	7
P0102	Positive	6

P0219	Negative	5
P0203	Positive	8
P0310	Positive	4
P0401	Positive	6
P0151	Negative	5

Accordingly, we evaluated polydactyly, syndactyly and radial polydactyly abnormalities by processing a total of 250 radiographs (150 normal, 100 abnormal) using the medial axis transformation technique. Forty patients were successfully detected as having polydactyly syndrome (having six, seven or eight fingers); 30 patients were detected as having syndactyly syndrome (having three or four fingers); and 30 patients were detected with radial polydactyly syndrome (having two or three branches in a finger). Others were detected as normal radiographs having five fingers. In Table 1, patients identified as P0712 and P0310 were detected as having syndactyly syndrome, with four- and three-finger digits. Moreover, P0901, P0529, P0102, P0203 and P0401 were determined to have polydactyly and radial polydactyly syndrome with six, seven, and eight fingers, respectively. P0786, P0219 and P0151 were shown to have normal, five-digit finger counts.

5.2. Results for Angle Computation between the Fingers

Subsequently, the detection of another hand deformity, the dislocation of the angles between the fingers were computed on 120 radiographs (70 normal and 50 abnormal). By using a mathematical formulation, angles are computed between each of the fingers with reference to the thumb. In Table 2, P0931 and P0832 have angles in the normal range. Among six patients—P0984, P0942, P0532, P0921, P0781 and P0877—a few of them had dislocations of the angles between the thumb and the little finger, the thumb and the ring finger, the thumb and the middle finger, and the thumb and the index finger. Moreover, two patients—P0952 and P0779—had abnormal angles between all the fingers, as the reference point of the thumb was dislocated from its mean position, making all the corresponding finger angles abnormal.

Table 2 Angle computation between the corresponding fingers

P_ID	Index to Thumb	Middle to Thumb	Ring to Thumb	Small to Thumb
P0931	20.821°	35.762°	44.621°	65.922°
P0984	23.321°	39.424°	48.234°	75.231°
P0952	65.234°	75.412°	86.211°	98.132°
P0942	19.452°	36.237°	53.342°	66.431°
P0532	18.421°	42.128°	51.312°	75.221°
P0921	23.121°	38.192°	51.923°	72.489°
P0832	24.133°	38.413°	47.821°	67.434°
P0781	27.341°	39.145°	52.712°	66.453°
P0877	23.173°	40.327°	52.431°	68.322°
P0779	26.321°	42.412°	53.344°	70.324°

5.3. Results for Missing Finger Phalanges

Missing phalange bones were computed on 190 hand radiographs. The circularity technique was carried out on 70 radiographs (40 normal and 30 abnormal) by selecting all the finger points and enclosing them in a shape. Thus, measuring the circularity of the region of interest in the hand in Table 3 represents three patients having a circularity near 1, meaning all the phalanges were present in the hand. Seven patients were categorized as abnormal, as the circularity of the hand region was not close to 1, which indicates a few missing phalange bones in the hand.

Table 3 Circularity result for the absence of finger phalanges

P_ID	Circularity of DIP	Status
P0312	0.7231 ≃ 0.7	Abnormal
P0421	0.8917 ≃ 0.9	Normal
P0413	0.6231 ≃ 0.6	Abnormal
P0234	0.6234 ≃ 0.6	Abnormal
P0545	0.4324 ≃ 0.4	Abnormal
P0866	0.9872 ≃ 1	Normal
P0967	0.5231 ≃ 0.5	Abnormal
P0346	0.9521 ≃ 1	Normal
P0984	0.6443 ≃ 0.6	Abnormal
P0454	0.545 ≃ 0.5	Abnormal

Additionally, the completeness of the phalanges in the hand radiograph was measured using a standard deviation formulation. First, the length of each of the fingers was calculated for 120 radiographs (60 normal and 60 abnormal); then, the mean standard deviation was computed for the little, ring, middle and index fingers, and thumb, respectively. Table 4 shows the absence of the little finger and ring finger phalanges of patient P1231, the middle finger phalanges of P2012 and P1231, the index finger phalanges of P2321 and the absence of the thumb phalanges of P1231 and P2455.

Table 4 Mean standard deviation for the absence of finger phalanges

Finger	P2012	P2321	P1932	P1231	P2455	S.D
Small	284	280	285	288	280	283 ± 3
Ring	333	330	340	342	331	335 ± 6

Continuation of Table 4

Middle	345	331	337	315	335	333± 11
Index	342	329	340	339	335	337

						± 7
Thumb	248	249	246	232	260	247 ± 9

5.4. Results for Finger Flexion from the Normal Trend

Finger bending or finger flexion from the normal trend was computed on 180 radiographs (100 normal and 80 abnormal) by using the morphological medial axis transformation technique to generate skeleton points and mathematical formulas to compute the linear line for each of the fingers. Subsequently, the distance from each skeleton point and linear line is measured using the distance formula. Fig. 11(a) indicates the thumb has a higher dispersion rate than the other four fingers, as it has deviated from its actual position.

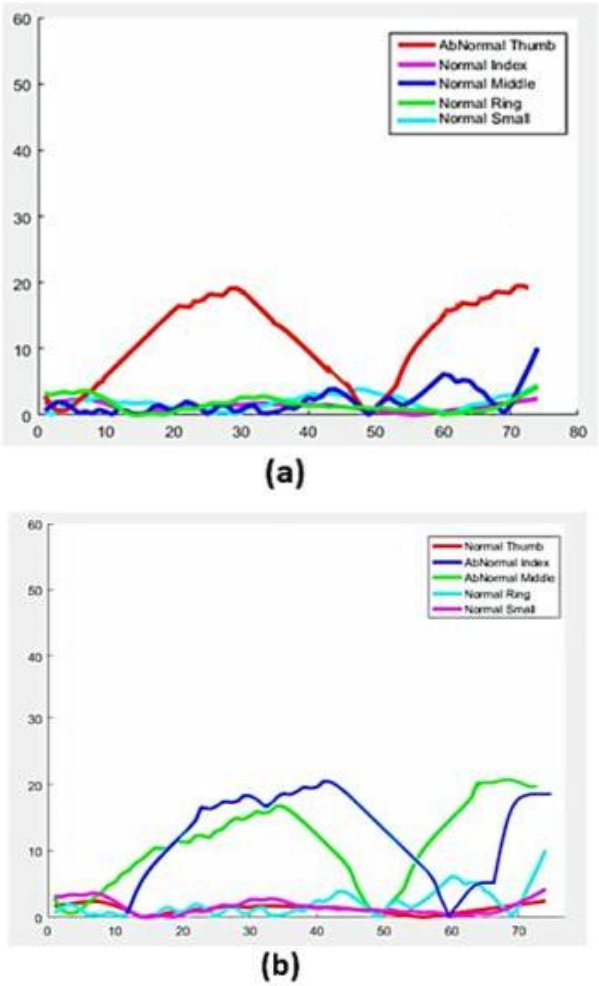

Fig. 11 Results for finger bending from the normal trend: (a) thumb bending from normal trend results, (b) index and middle finger bending from normal trend results

5.5. Results for Fracture Computation

Fractures were computed on 210 radiographs (120 normal, 90 abnormal) carrying different bone breakages including breakages in the carpal wrist bone and the metacarpal bone and many in the phalanges.

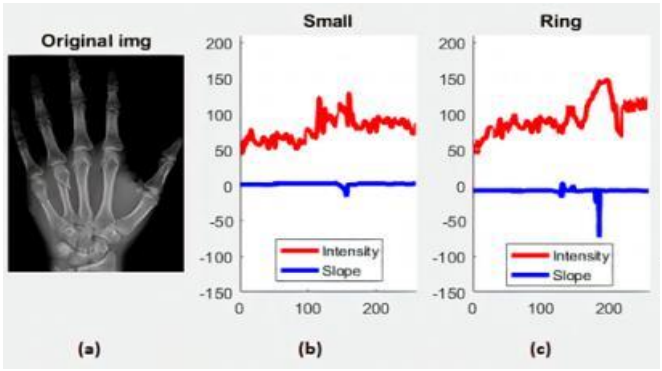

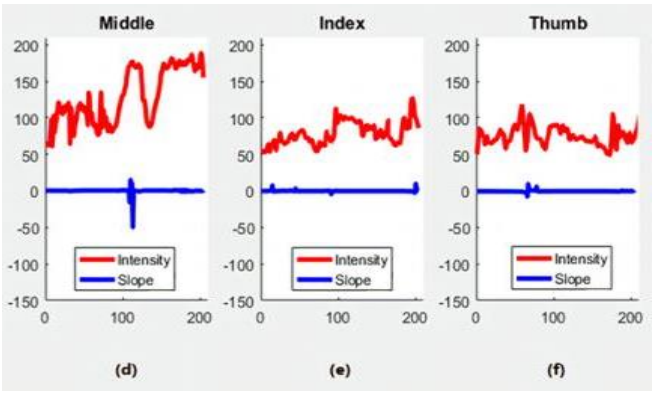

Fig. 12 Results for middle finger fracture: (a) represents original radiograph; (b), (c), (e), and (f) represent the slight change of intensity exhibiting normal finger gap with no change in slope. However, (d) represents a big change in intensity and slope changes abruptly, which indicates the middle finger's breakage of the proximal interphalangeal bone

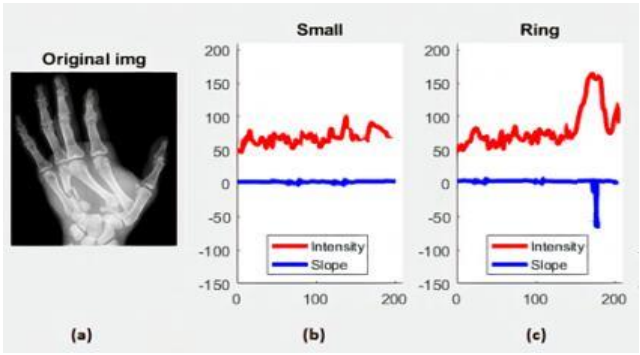

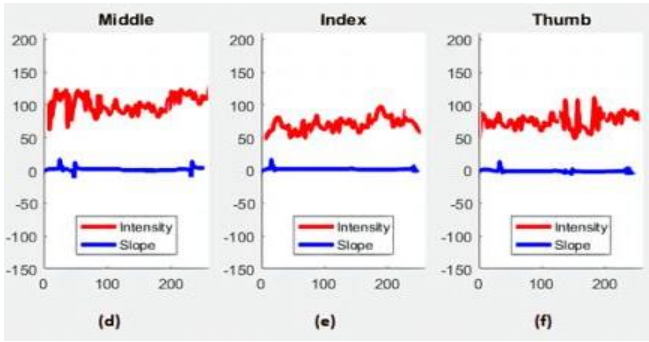

Fig. 13: Results for the metacarpal bone of the ring finger fracture: (a) original radiograph, (b), (d), (e), and (f) the slight change of intensity exhibiting normal finger gap whereas there is no change in slope in small, middle, index fingers, and thumb. However, (c) represents a drastic change in intensity and slope, which indicates the breakage of the fourth metacarpal bone of the ring finger

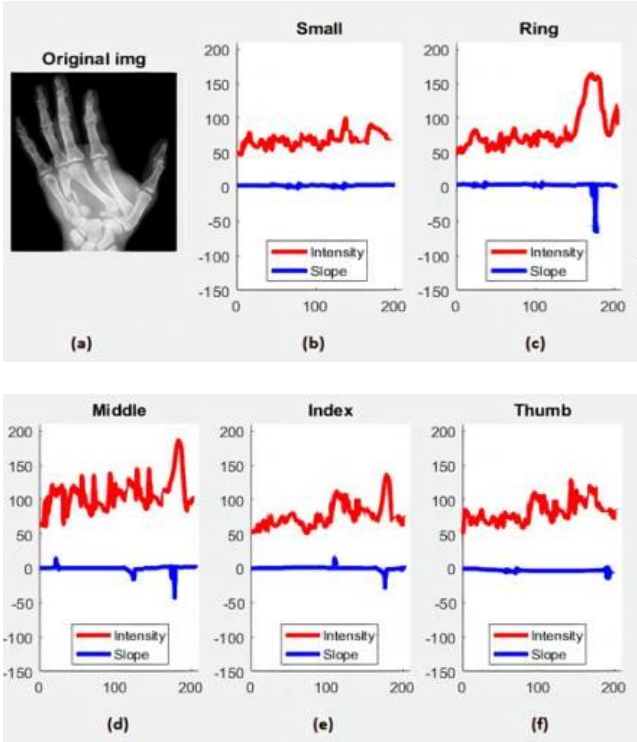

Fig. 14 Results for the metacarpal bone of ring, middle, and index finger fracture: (a) Original radiograph, (b) and (f) show the slight change of intensity exhibiting normal finger gap whereas there is no change in slope in the small finger and thumb. However, (c), (d), (e) represent a drastic change in intensity as well as slope which indicates breakage of the second, third, and fourth metacarpal bones of the index, middle, and ring fingers

6. Discussion

The prime purpose of this research was to automatically detect different hand abnormalities at an early stage by analyzing a total of 950 hand radiographs. Among them, 910 radiographs were successfully categorized as normal or abnormal. Inclusively, 245 out of 250 radiographs detected the enumeration of the finger count, 110 out of 120 detected the angle computation between the fingers, 180 out of 190 detected missing phalanges, 175 out of 180 detected finger flexion from the normal trend and 200 out of 210 were utilized for fracture computation.

$$\text{Accuracy} = \frac{\text{TN+TP}}{\text{TP+FP+TN+FN}} \quad (9)$$

$$\text{Precision} = \frac{\text{TP}}{\text{FP+TP}} \quad (10)$$

$$\text{Recall} = \frac{\text{TP}}{\text{FN+TP}} \quad (11)$$

$$\text{Sensitivity} = \frac{\text{TP}}{\text{FN+TP}} \quad (12)$$

$$\text{Specificity} = \frac{\text{TN}}{\text{FP+TN}} \quad (13)$$

Therefore, the performance of the system can be visualized by the evaluation of the confusion matrix in Fig. 15. The total performance accuracy of the system in successfully detecting abnormalities in hand radiographs is 95.95 percent, as specified in Equation (9). The patients having abnormalities which were successfully detected as TP are evaluated using precision in Equation (10); 95.69% of positive radiographs were detected. The recall, depending upon TP estimated values over the sum of FN and TP, is 94.78 percent. Subsequently, the F1-score, measured to evaluate the total degree of accuracy of precision and recall, is 95.23 percent; the sensitivity and specificity of the system are 94.78 percent and 96.83 percent, as expressed in Equations (11), (12) and (13), respectively. Moreover, the receiver operating characteristics curve indicates the efficiency of the system, with the true positive rate and false positive rate near 1.

Table 5 Performance of passed and detected images

	Enumeration of Fingers	Angle computation between Fingers	Missing of Phalanges	Finger flexion from the normal trend	Fracture detection	Total
No: of images passed	250	120	190	180	210	950
No: of images successfully detected as normal/abnormal	245	110	180	175	200	910

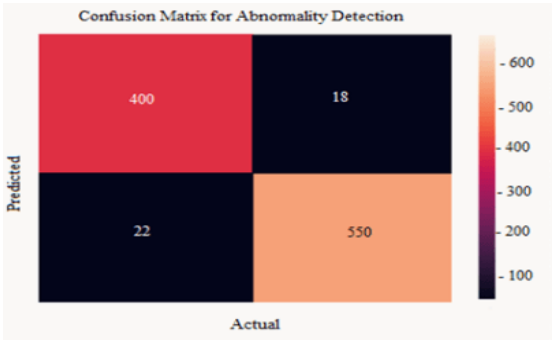

Fig. 15 Confusion matrix for visualizing the performance

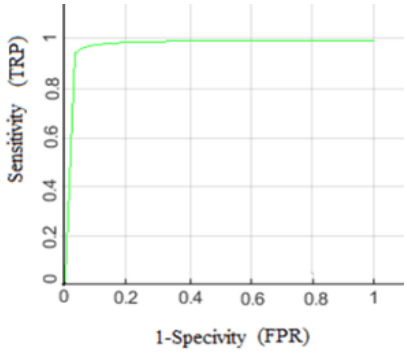

Fig. 16 ROC curve

References

[1] HARRIS-ADAMSON C., EISEN E. A., KAPELLUSCH J., GARG A., HEGMANN K. T., THIESE M. S., DALE A. M., EVANOFF B., BURT S., BAO S., and SILVERSTEIN B. Biomechanical risk factors for carpal tunnel syndrome: a pooled study of 2474 workers. *Occupational and Environmental Medicine*, 2015, 72(1): 33-41. https://doi.org/10.1136/oemed-2014-102378

[2] FEIX T., ROMERO J., SCHMIEDMAYER H. B., DOLLAR A. M., and KRAGIC D. The grasp taxonomy of human grasp types. *IEEE Transactions on Human-Machine Systems*, 2015, 46(1): 66-77. https://doi.org/10.1109/THMS.2015.2470657

[3] SANDVALL B. K., KEYS K. A., and FRIEDRICH J. B. Severe hand injuries from fireworks: injury patterns, outcomes, and fireworks types. *The Journal of Hand Surgery*, 2017, 42(5): 385.E1-385.E8. https://doi.org/10.1016/j.jhsa.2017.01.028

[4] GOLDFARB C. A., SHAW N., STEFFEN J. A., and WALL L. B. The Prevalence of Congenital Hand and Upper Extremity Anomalies Based Upon the New York Congenital Malformations Registry. *Journal of Pediatric Orthopaedics*, 2017, 37(2): 144-148. https://doi.org/10.1097/BPO.0000000000000748
[5] BENJAMIN H. J., & HANG B. T. Common acute upper extremity injuries in sports. *Clinical Pediatric Emergency Medicine*, 2007, 8(1): 15-30. https://doi.org/10.1016/j.cpem.2007.02.003
[6] ZARE M. R., MUEEN A., SENG W. C., and AWEDH M. H. Combined feature extraction on medical x-ray images. Proceedings of the 3rd International Conference on Computational Intelligence, Communication Systems and Networks, Bali, 2011, pp. 264-268. https://doi.org/10.1109/cicsyn.2011.63
[7] CHAI H. Y., WEE L. K., SWEE T. T., and HUSSAIN S. Gray-level co-occurrence matrix bone fracture detection. *WSEAS Transactions on Systems*, 2011, 10(1): 7-16. https://doi.org/10.3844/ajassp.2011.26.32
[8] AL-AYYOUB M., HMEIDI I., and RABABAH H. Detecting Hand Bone Fractures in X-Ray Images. *Journal of Multimedia Processing and Technologies*, 2013, 4(3): 155-168. https://dline.info/jmpt/fulltext/v4n3/1.pdf
[9] AL-AYYOUB M., & AL-ZGHOOL D. Determining the type of long bone fractures in x-ray images. *WSEAS Transactions on Information Science and Applications*, 2013, 10(8): 261-270. https://www.wseas.org/multimedia/journals/information/2013/b065705-278.pdf
[10] BHISIKAR S. A., & KALE S. N. Automatic joint detection and measurement of joint space width in arthritis. Proceedings of the IEEE International Conference on Advances in Electronics, Communication and Computer Technology, Pune, 2016, pp. 429-432. https://doi.org/10.1109/ICAECCT.2016.7942626
[11] TRIPATHI A. M., UPADHYAY A., RAJPUT A. S., SINGH A. P., and KUMAR B. Automatic detection of fracture in femur bones using image processing. Proceedings of the International Conference on Innovations in Information, Embedded and Communication Systems, Coimbatore, 2017, pp. 1-5. https://doi.org/10.1109/ICIIECS.2017.8275843
[12] JOHARI N., & SINGH N. Bone fracture detection using edge detection technique. In: PANT M., RAY K., SHARMA T., RAWAT S., and BANDYOPADHYAY A. (eds.) *Soft Computing: Theories and Applications. Advances in Intelligent Systems and Computing*, Vol. 584. Singapore: Springer, pp. 11-19. https://doi.org/10.1007/978-981-10-5699-4_2
[13] RAJPURKAR P., IRVIN J., BAGUL A., DING D., DUAN T., MEHTA H., YANG B., ZHU K., LAIRD D., BALL R. L., and LANGLOTZ C. MURA: Large dataset for abnormality detection in musculoskeletal radiographs. https://arxiv.org/pdf/1712.06957.pdf
[14] YANG X., SHEN X., LONG J., and CHEN H. An improved median-based Otsu image thresholding algorithm. *AASRI Procedia*, 2012, 3: 468-473. https://doi.org/10.1016/j.aasri.2012.11.074
[15] NARUSE T., TAKAHARA M., TAKAGI M., and OGINO T. Early morphological changes leading to central polydactyly, syndactyly, and central deficiencies: an experimental study in rats. *The Journal of Hand Surgery*, 2007, 32(9): 1413-1417. https://doi.org/10.1016/j.jhsa.2007.06.017
[16] AMENTA N., CHOI S., and KOLLURI R. K. The power crust, unions of balls, and the medial axis transform. *Computational Geometry*, 2001, 19(2-3): 127-153. https://doi.org/10.1016/s0925-7721(01)00017-7
[17] CHEN W., SUI L., XU Z., and LANG Y. Improved Zhang-Suen thinning algorithm in binary line drawing applications. Proceedings of the International Conference on Systems and Informatics, Yantai, 2012, pp. 1947-1950. https://doi.org/10.1109/icsai.2012.6223430
[18] JAWAS N., & SUCIATI N. Image inpainting using erosion and dilation operation. *International Journal of Advanced Science and Technology*, 2013, 51: 127-134. https://article.nadiapub.com/IJAST/vol51/10.pdf
[19] STIDHAM R. W., ENCHAKALODY B., WALJEE A. K., HIGGINS P. D., WANG S. C., SU G. L., WASNIK A. P., and AL-HAWARY M. Assessing Small Bowel Stricturing and Morphology in Crohn's Disease Using Semi-Automated Image Analysis. *Inflammatory Bowel Diseases*, 2020, 26(5): 734-742. https://doi.org/10.1093/ibd/izz196
[20] HIRAI Y., YOSHIDA K., YAMANAKA K., INOUE A., YAMAKI K. I., and YOSHIZUKA M. An anatomic study of the extensor tendons of the human hand. *The Journal of Hand Surgery*, 2001, 26(6): 1009-1015. https://doi.org/10.1016/S0363-5023(01)70045-7
[21] CHEN F. C., APPENDINO S., BATTEZZATO A., FAVETTO A., MOUSAVI M., and PESCARMONA F. Constraint study for a hand exoskeleton: human hand kinematics and dynamics. *Journal of Robotics*, 2013, 2013: 910961. https://doi.org/10.1155/2013/910961
[22] KELAIN M. J. Compatibility of Enhancement and Segmentation of Digital Image Processing in Medical Applications. *Journal of Southwest Jiaotong University*, 2020, 55(1). https://doi.org/10.35741/issn.0258-2724.55.1.50

参考文:

[1] HARRIS-ADAMSON C. 、EISEN E. A. 、KAPELLUSCH J. 、GARG A. 、HEGMANN K. T. 、THIESE M. S.、DALE A. M.、EVANOFF B.、BURT S.、BAO S. 和 SILVERSTEIN B. 腕骨的生物力学风险因素隧道综合症：对 2474 名工人的汇总研究。职业与环境医学, 2015, 72(1): 33-41。https://doi.org/10.1136/oemed-2014-102378
[2] FEIX T.、ROMERO J.、SCHMEDMAYER H. B.、DOLLAR A. M. 和 KRAGIC D. 人类抓握类型的抓握分类法。IEEE 人机系统汇刊，2015，46(1)：66-77。https://doi.org/10.1109/THMS.2015.2470657
[3] SANDVALL B. K.、KEYS K. A. 和 FRIEDRICH J. B. 烟花造成的严重手部损伤：损伤模式、结果和烟花类型。手外科杂志，2017，42(5)：385.E1-385.E8 。https://doi.org/10.1016/j.jhsa.2017.01.028
[4] GOLDFARB C. A.、SHAW N.、STEFFEN J. A. 和 WALL L. B. 基于纽约先天性畸形登记处的先天性手部和上肢畸形的患病率。儿科骨科杂志，2017，37（2）：144-148。https://doi.org/10.1097/BPO.0000000000000748
[5] BENJAMIN H. J., & HANG B. T. 运动中常见的急性上肢损伤。临床儿科急诊医学，2007，8(1)：15-30. https://doi.org/10.1016/j.cpem.2007.02.003
[6] ZARE M. R.、MUEEN A.、SENG W. C. 和 AWEDH M. H. 医学 X 射线图像上的组合特征提取。第三届计算

智能、通信系统和网络国际会议论文集，巴厘岛，2011，第 264-268 页。https://doi.org/10.1109/cicsyn.2011.63
[7] CHAI H. Y.、WEE L. K.、SWEE T. T. 和 HUSSAIN S. 灰度共生基质骨折检测。WSEAS 系统交易，2011，10(1)：7-16。 https://doi.org/10.3844/ajassp.2011.26.32
[8] AL-AYYOUB M.、HMEIDI I. 和 RABABAH H. 在 X 射线图像中检测手骨骨折。多媒体处理与技术杂志，2013，4(3)：155-168。https://dline.info/jmpt/fulltext/v4n3/1.pdf
[9] AL-AYYOUB M., & AL-ZGHOOL D. 确定 X 射线图像中长骨骨折的类型。WSEAS 信息科学与应用汇刊，2013，10(8)：261-270。https://www.wseas.org/multimedia/journals/information/2013/b065705-278.pdf
[10] BHISIKAR S. A., & KALE S. N. 关节炎中关节间隙宽度的自动检测和测量。IEEE 电子、通信和计算机技术进展国际会议论文集，浦那，2016，第 429-432 页。https://doi.org/10.1109/ICAECCT.2016.7942626
[11] TRIPATHI A. M.、UPADHYAY A.、RAJPUT A. S.、SINGH A. P. 和 KUMAR B. 使用图像处理自动检测股骨骨折。信息、嵌入式和通信系统创新国际会议论文集，哥印拜陀，2017，第 1-5 页。https://doi.org/10.1109/ICIIECS.2017.8275843
[12] JOHARI N., & SINGH N. 使用边缘检测技术进行骨折检测。在：PANT M.、RAY K.、SHARMA T.、RAWAT S. 和 BANDYOPADHYAY A.（编辑）软计算：理论和应用。智能系统和计算进展，卷。 584. 新加坡：斯普林格，第 11-19 页。 https://doi.org/10.1007/978-981-10-5699-4_2
[13] RAJPURKAR P.、IRVIN J.、BAGUL A.、DING D.、DUAN T.、MEHTA H.、YANG B.、ZHU K.、LAIRD D.、BALL RL 和 LANGLOTZ C. 村：大型数据集用于肌肉骨骼 X 光片的异常检测。https://arxiv.org/pdf/1712.06957.pdf
[14] YANG X., SHEN X., LONG J., 和 CHEN H. 一种改进的基于中值的大津图像阈值算法。AASRI 序曲, 2012, 3: 468-473。https://doi.org/10.1016/j.aasri.2012.11.074
[15] NARUSE T.、TAKAHARA M.、TAKAGI M. 和 OGINO T. 导致中枢多指、并指和中枢缺陷的早期形态学变化：大鼠实验研究。手外科杂志, 2007, 32(9): 1413-1417。 https://doi.org/10.1016/j.jhsa.2007.06.017
[16] AMENTA N.、CHOI S. 和 KOLLURI R. K. 力量外壳、球的联合和中轴变换。计算几何，2001，19(2-3)：127-153。 https://doi.org/10.1016/s0925-7721(01)00017-7
[17] CHEN W., SUI L., XU Z., 和 LANG Y. 在二进制线画应用中改进的张孙细化算法。国际系统与信息学会议论文集，烟台，2012，1947-1950 页。https://doi.org/10.1109/icsai.2012.6223430
[18] JAWAS N., & SUCIATI N. 使用腐蚀和膨胀操作的图像修复。国际先进科学技术杂志，2013，51：127-134。https://article.nadiapub.com/IJAST/vol51/10.pdf
[19] STIDHAM R. W.、ENCHAKALODY B.、WALJEE A. K.、HIGGINS P. D.、WANG S. C.、SU G. L.、WASNIK A. P. 和 AL-HAWARY M. 使用半自动图像分析评估克罗恩病中的小肠狭窄和形态学。炎症性肠病，2020, 26(5): 734-742。https://doi.org/10.1093/ibd/izz196
[20] HIRAI Y.、YOSHIDA K.、YAMANAKA K.、INOUE A.、YAMAKI K. I. 和 YSHIZUKA M. 人手伸肌腱的解剖学研究。手外科杂志, 2001, 26(6): 1009-1015。https://doi.org/10.1016/S0363-5023(01)70045-7
[21] CHEN F. C.、APPENDINO S.、BATTEZZATO A.、FAVETTO A.、MOUSAVI M. 和 PESCARMONA F. 手部外骨骼的约束研究：人类手部运动学和动力学。 机器人学杂志，2013，2013：910961。https://doi.org/10.1155/2013/910961
[22] KELAIN M. J. 医学应用中数字图像处理增强和分割的兼容性。西南交通大学学报，2020, 55(1). https://doi.org/10.35741/issn.0258-2724.55.1.50